Hindawi
Geofluids
Volume 2022, Article ID 2379040, 15 pages
https://doi.org/10.1155/2022/2379040

Research Article

Research on the Extraction Technology of Gas-Integrated Working-Face in Close Coal Seam Mining in Permafrost Area

Chao Wu[1] **and Rongbin Deng**[2]

[1]*Yuncheng Vocation and Technical University, Yuncheng 044000, China*
[2]*Chongqing Shanhe Ecological Environment Engineering Co., Ltd., Chongqing 400000, China*

Correspondence should be addressed to Chao Wu; 553493195@qq.com

Received 27 December 2021; Revised 19 April 2022; Accepted 13 May 2022; Published 4 July 2022

Academic Editor: Shijin Li

In order to understand the mechanical deformation characteristics of the permafrost layer and the stress-fracture-gas seepage law of the superimposed mining of the proximity coal seam group, a coupled gas-solid model of the proximity coal seam in the permafrost area was constructed based on the theoretical model of small deflection of thin plate and the deformation control equation, gas transport equation, porosity evolution equation and permeability evolution equation of the coal rock body, and the analysis of the dependent project. The analysis was carried out at the NMT coal mine. The results show that the multiyear permafrost seam in the NMT coal mine has a tendency to move to the left and will produce extensive pull damage near the right end. The initial and periodic collapse steps are 192.87 m and 43.24 m, respectively; the pore and fissure structural characteristics of the NMT coal seam are not conducive to gas transport, and the stress and fissure fields have a nonlinear increasing effect. The study also proposed the "protected seam mining and bottom extraction lane directional drilling group comining technology" to increase the daily production of working face by 25.8%. The results of the study can be used as a reference for similar projects.

1. Introduction

The complex permafrost geological environment has caused a large number of damage problems in the permafrost layer due to freezing, which seriously threatens the safe and efficient mining of coal fields and makes the control work more difficult than ever [1, 2]. Xu et al. based on a large number of experimental studies and the summary of previous research results comprehensively analyzed and studied the influence of the main factors [3]. The study through the study of the weak interlayer in the Dajiang River of the Gezhouba Project puts forward some types of microstructures of the weak interlayer [4]. The relationship between ground stress and the physical and mechanical parameters of the weak layer zone was studied in the study, taking the weak interlayer at a hydroelectric dam site on the Jinsha River as an example, and it was concluded that ground stress is the most active factor controlling the engineering properties of the weak layer zone; the effect of freeze-thaw cycles on the shear strength properties of lime powder soils was discussed in the study [5, 6]. The relationship between the physical and mechanical parameters of the weak layer zone and the physical and mechanical parameters of the weak layer zone was studied in the study [7]. The mechanical properties of soils change before and after freeze-thawing, and the main reason for the change in soil mechanical properties due to repeated freeze-thawing is the change in soil structure, i.e., the destruction of the linkage between soil particles and the rearrangement of soil particles [8–12]. In summary, little research has been reported on the mechanical properties of coal mines, especially in high-altitude permafrost. Therefore, it is of practical importance to research the mechanical properties of strata in high-altitude permafrost areas. Close coal seam groups are widely distributed in China, with small

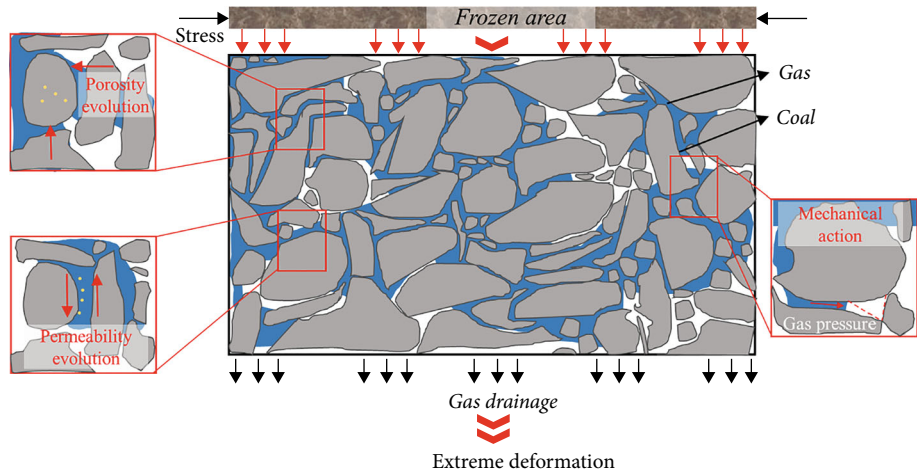

Figure 1: Schematic diagram of the coupling model.

seam spacing and large interaction between seams, and coal seam gas is always a threat to mine safety during mining. As the mining depth continues to increase, the gas content and pressure of the coal seam increases, making it more difficult to manage the gas. In the area of close coal seam group: the study explored the stress-fracture evolution characteristics of the close coal seam group under superposition mining conditions and realized the refined simulation of the distribution characteristics of the mining fracture zone [13, 14]. Qi et al. studied the mining influence range of the first mining layer under protective layer mining and analyzed the feasibility of the protective layer mining technology of the high gas coal seam group [15]. Ma et al. found that the overburden collapse characteristics under superposition mining conditions [16]. The scholars studied the spatial and temporal evolution characteristics of the three-dimensional stress field and the fracture mechanics behavior of the overburdened fracture zone under repeated mining of coal seam clusters [17, 18]. In the area of coal and gas comining: literature initially puts forward the new concept of "green mining" [19, 20]. Literature studied the fracture mechanism and fractal characteristics of the overlying rock layer and revealed the evolution law of mining fractures [21–24]. Papers changed the traditional "wind drainage" gas management measures and adopted pressure relief mining in the first mining layer to achieve a new model of efficient "extraction" of gas and formed a coal and gas comining technology under protective layer mining [25]. Papers established the theory of efficient coal and gas comining under coal pillarless mining and achieved a quantitative description of coal seam gas [26–29]. A large-aperture kilometer directional drilling rig was used to efficiently extract gas from the fissure zone of the roof, and the mechanism of coal and gas comining in kilometer directional drilling in high-gas coal seams was proposed [30, 31]. The nonlinear characteristics and failure characteristics of coal energy evolution under different gas pressures are studied [32].

The above research results have effectively solved the technical problems that exist in the mining process of close coal seam clusters and constitute the basic content of coal and gas comining technology in China, but there is less research in the direction of the coupling mechanism of the stress field and gas pressure under the mining conditions of close coal seam clusters. Based on this, this paper takes the NMT mine as the research background and investigates the stress field and gas pressure crystallization under the superimposed mining conditions in the mine, to provide theoretical support for the coal and gas comining technology under the close coal seam group conditions.

2. Theoretical Model

Assumptions: coal is a porous medium consisting of pores-fissures with nonuniformity, anisotropy, and discontinuity, and also considering the characteristics of large depth of gas deposit, coal is taken as the object of study to analyze the gas extraction characteristics of proximity coal seam mining, and the following assumptions are made [33].

(1) It is assumed that the coal rock mass is an isotropic homogeneous linear elastic material

(2) The coal seam gas adsorption model conforms to the Langmuir equation and the gas flow satisfies Darcy's law

(3) The gas is at a constant temperature and the transport and diffusion of a gas is an isothermal process

Coupling model: based on the above assumptions, a gas-solid coupling model is constructed. It is shown as Figure 1.

2.1. Deformation and Mechanical Characteristics of Permafrost Coal (Rock) Seams. A permafrost environmental coal (rock) seam, subject to temperature loading, can be decomposed into two components, longitudinal load stress acting between the layers and a transverse load stress perpendicular to the midplane. For the longitudinal load stresses, they can be considered to be analyzed uniformly

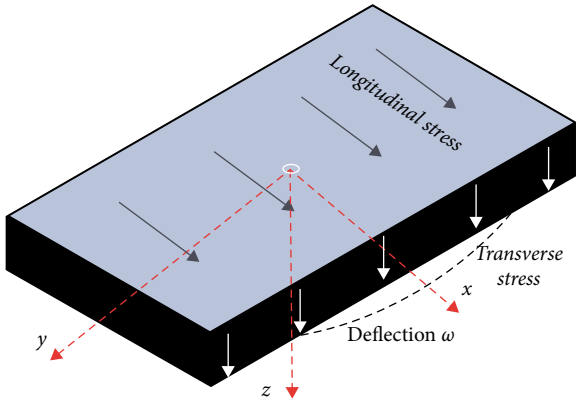

Figure 2: Temperature loading in the permafrost zone.

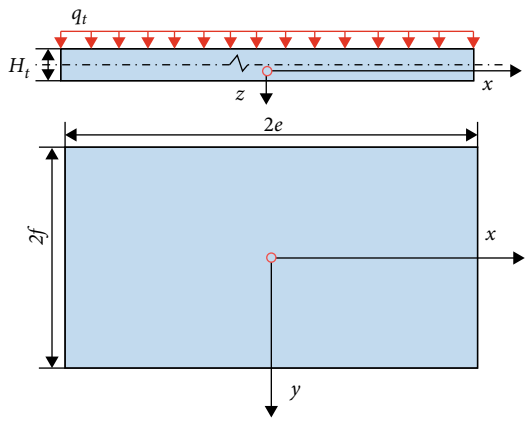

Figure 3: Mechanical model of initial permafrost break.

along the thickness direction, and therefore, the stresses, strains, and displacements caused by them can be calculated by solving for the plane stress problem. As shown in Figure 2, the transverse loads will cause the sheet to bend, and the stresses, strains, and displacements caused can be calculated as a sheet bending problem. In the thin plate bending, the plane bent into the surface, known as the elastic surface of the thin plate, and the point in the surface perpendicular to the plane, along the z -direction of displacement, is called the deflection ω.

Because the thickness of the coal (rock) seam is much less than the planar dimension, the Kirchhoff hypothesis is invoked to establish a theoretical model for small deflections in thin slabs.

(1) There is no deformation in the midplane of the plate, i.e., the midplane bends to a neutral surface during bending. It follows that εz, γzx, and γzy are negligible. This leads to the following:

$$\omega = \omega(x, y), \tag{1}$$

where ε is a positive strain; γ is the shear strain; and ω is the deflection

(2) The deformation caused by the strain component εz can be disregarded. By this assumption and in combination with assumption Equation (1), the physical Equation (2) for the small deflection of a thin plate can be obtained

$$\begin{cases} \varepsilon_x = \dfrac{1}{E}\left(\sigma_x - \upsilon\sigma_y\right), \\ \varepsilon_y = \dfrac{1}{E}\left(\sigma_y - \upsilon\sigma_x\right), \\ \gamma_{xy} = \dfrac{2(1+\upsilon)}{E}\tau_{xy}, \end{cases} \tag{2}$$

where E is the modulus of elasticity; υ is the Poisson's ratio

(3) The points in the plane have no displacement parallel to the midplane. That is, when $z = 0$, $u = 0$, and $v = 0$, i.e., $\varepsilon x = 0$, $\varepsilon y = 0$, and $\gamma xy = 0$, then the differential equation for the elastic surface of a thin plate with a small deflection problem Equation (3), i.e., the basic equation of the problem, can be obtained

$$\frac{Eh^3}{12(1-\upsilon^2)}\nabla^4\omega = q, \tag{3}$$

where q is the transverse load on the thin plate; h is the thickness of the thin plate; ∇ is the Laplace operator, $\nabla^4\omega = ((\partial^4\omega/\partial x^4) + 2(\partial^4\omega/\partial x^2\partial y^4) + (\partial^4\omega/\partial y^4))$.

This gives the relationship between the cross-sectional internal force of the thin plate and the deflection of the thin plate, and the parametric elimination of the deflection gives Equations (4) and (5). From this, each stress extreme and its corresponding location can be found. In solving the multiyear permafrost deformation and damage problem, the load-induced bending and torsional stresses are numerically larger and are the main stresses; transverse shear stresses are numerically relatively small and are secondary stresses; extrusion stresses are numerically smaller and are more secondary stresses. Therefore, when solving thin-slab problems with multiyear permafrost layers, the focus is on solving for the major internal forces, i.e., bending moments and torsional moments.

At the start of the coal seam excavation, before the initial break of the multiyear permafrost seam with the coal seam group, the mining mechanics analysis model is a thin plate surrounded by solid coal rock-solid support; the mechanical calculation model is shown in Figure 3. In the figure, $2e$ is the length of the permafrost layer, and $2f$ is the width of the permafrost layer. The damage forces in the vertical direction are mainly caused by their own gravity G. The uniform load q_t is the perennial permafrost capacity.

$$\begin{cases} M_x = -D\left(\dfrac{\partial^2\omega}{\partial x^2} + \nu\dfrac{\partial^2\omega}{\partial y^2}\right), \\ M_y = -D\left(\dfrac{\partial^2\omega}{\partial y^2} + \nu\dfrac{\partial^2\omega}{\partial x^2}\right), \\ M_{xy} = M_{xy} = -D(1-\nu)\dfrac{\partial^2\omega}{\partial x\partial y}, \\ Q_x = -D\dfrac{\partial}{\partial x}\nabla^2\omega, \\ Q_y = -D\dfrac{\partial}{\partial y}\nabla^2\omega, \end{cases} \tag{4}$$

$$\begin{cases} \sigma_x = \dfrac{12M_x}{h^3}z, \\ \sigma_y = \dfrac{12M_y}{h^3}z, \\ \sigma_z = -2q\left(\dfrac{1}{2} - \dfrac{z}{h}\right)^2\left(1 + \dfrac{z}{h}\right), \\ \tau_{xy} = \tau_{yx} = \dfrac{12M_{xy}}{h^3}z, \\ \tau_{xz} = \dfrac{6Q_x}{h^3}\left(\dfrac{h^2}{4} - z^2\right), \\ \tau_{yz} = \dfrac{6Q_y}{h^3}\left(\dfrac{h^2}{4} - z^2\right). \end{cases} \tag{5}$$

The boundary conditions at this point are $[\partial\omega/\partial x]_{x\pm c}{}^{(\omega)_{x=\pm e}=0} = 0\,[\partial\omega/\partial x]_{x+\pm}{}^{(\omega)_{x=\pm f}=0} = 0$.

Using an approximate solution, assume that the deflection function of the perennial permafrost "slab cover" is

$$\omega = A\left(x^2 - e^2\right)^2\left(y^2 - f^2\right)^2. \tag{6}$$

Taking the partial derivatives of x and y, respectively, yields

$$\begin{aligned} \frac{\partial\omega}{\partial x} &= 4Ax\left(x^2 - e^2\right)^2\left(y^2 - f^2\right)^2, \\ \frac{\partial\omega}{\partial y} &= 4Ay\left(x^2 - e^2\right)^2\left(y^2 - f^2\right)^2. \end{aligned} \tag{7}$$

Based on the principle of minimum potential energy for bending of thin plates, the Galyagin method was used to determine the coefficient A, $A = (49 \cdot q_t)/(128 \cdot (7e^4 + 4e^2f^2 + 7f^4))$.

The equation for the deflection surface of a four-sided solidly supported perennial permafrost "slab cover" is

$$\omega = \frac{49q_1}{128\left(7e^4 + 4e^2f^2 + 7f^4\right)}\left(x^2 - e^2\right)^2\left(y^2 - f^2\right)^2. \tag{8}$$

From this, the parameters M_x, M_y, M_{xy}, Q_x, Q_y, etc. can be calculated, where M_x and M_y are

$$\begin{aligned} M_x &= -\frac{7q_t}{32\left(e^4 + (4/7)e^2f^2 + f^4\right)}\left[\left(3x^2 - e^2\right)\left(y^2 - f^2\right)^2 + \upsilon\left(x^2 - e^2\right)\left(3y^2 - f^2\right)^2\right], \\ M_x &= -\frac{7q_t}{32\left(e^4 + (4/7)e^2f^2 + f^4\right)}\left[\left(3y^2 - e^2\right)\left(x^2 - f^2\right)^2 + \upsilon\left(y^2 - e^2\right)\left(3x^2 - f^2\right)^2\right]. \end{aligned} \tag{9}$$

From Equation (9), the perennial permafrost layer "plate cover" M_x, M_y bending moment maximum can be determined, when $x = \pm e$ on, $y = 0$, $(M_x)_{\max}$ for Equation (10); $y = \pm f$ on, $x = 0$, $(M_y)_{\max}$ for Equation (11).

$$(M_x)_{\max} = -\frac{7q_t}{16\left(e^4 + (4/7)e^2f^2 + f^4\right)}e^2f^4, \tag{10}$$

$$\left(M_y\right)_{\max} = -\frac{7q_t}{16\left(e^4 + (4/7)e^2f^2 + f^4\right)}e^4f^2. \tag{11}$$

Equation (10) and Equation (11) show that the bending moment reaches its maximum value at the midpoint of the long solid support and at the midpoint of the short solid support in the permafrost layer "slab cover." As the stresses in the section are proportional to the bending moment, it can be concluded that the positive stresses at the midpoint of the long solid support and at the midpoint of the short solid support also reach their maximum values at the section $z = \pm H_t/2$, i.e., the positive stresses on the upper and lower sides of the plate reach their maximum values in

$$\begin{aligned} (\sigma_x)_{\max} &= \frac{42q_x}{16\left(e^4 + (4/7)e^2f^2 + f^4\right)h^2}e^2f^4, \\ \left(\sigma_y\right)_{\max} &= \frac{42q}{16\left(e^4 + (4/7)e^2f^2 + f^4\right)h^2}e^4f^2. \end{aligned} \tag{12}$$

The peak point of the positive stress caused by the bending moment on both the long and short sides is located at the midpoint of each side of the permafrost "slab cover," and the bending moment at the midpoint of the long side is much greater than that at the midpoint of the short side, which means that the four-sided fixed permafrost "slab cover" should be at the middle of the upper surface of the long side. This means that the permafrost "cover" is most likely to break in the middle of the working face.

The permafrost layer is a brittle material with low tensile strength, so the bending deformation before the permafrost layer breaks is small. When the longitudinal load reaches the critical load for the flexure of the thin plate, if it is only the effect of the longitudinal load, a slight increase in the load at this time will make the displacement and internal force increase a lot, while in fact, the presence of the transverse load makes the displacement and internal force of the plate increase a lot, which eventually leads to the breakage of the permafrost layer. The rupture will be a tensile rupture dominated by buckling instability. When the maximum

tensile stress at a certain point in the permafrost layer reaches the permafrost tensile strength, the permafrost will fracture at that point, and the breaking conditions will be

$$\sigma_{\max} \geq \sigma_t, \tag{13}$$

where $\sigma_{\max}$ is the maximum principal stress in the permafrost; σ_t is the tensile strength limit of the permafrost.

As a result of the above analysis, the permafrost "slab cover" is prone to tensile damage on both sides of the inclined direction. In the vertical direction, the permafrost "slab cover" is subjected to its own gravity, and due to the movement deformation off-layer cracks between the protective rock beam and the permafrost "slab cover," the permafrost "slab cover" will deform following plate mechanics. In addition, after the coal seam has been mined, the perennial permafrost layer will have a significant overhang in one direction, at which point the perennial permafrost layer "plate cover" is highly susceptible to significant plastic deformation on both sides. The deformation results in a state where the left and right sides become simply supported and the front and rear sides are solidly supported, the mechanical model is shown in Figure 4.

The boundary conditions at this point are shown as follows.

$$\begin{aligned} (\omega)_{\substack{x=0 \\ x-2e}} &= 0 \left[\frac{\partial^2 \omega}{\partial x^2}\right]_{\substack{x=0 \\ x-2e}} = 0, \\ (\omega)_{x=\pm f} &= 0 \left[\frac{\partial \omega}{\partial y}\right]_{x=\pm f} = 0. \end{aligned} \tag{14}$$

The deflection function is obtained by Levy's solution as

$$\begin{aligned} \omega = \frac{64 q_t e^4}{\pi^5 D} \sum_{m=1,3,5,\ldots}^{\infty} \frac{1}{m^5} \Bigg[1 - \frac{(a_m cha_m + sha_m) ch(m\pi y/a)}{cha_m (a_m cha_m + sha_m) - a_m sh^2 a_m} \\ + \frac{sha_m}{cha_m (a_m cha_m + sha_m) - a_m sh^2 a_m} \\ \cdot \frac{m\pi y}{2e} sh \frac{m\pi y}{a} \Bigg] \sin \frac{m\pi x}{2e}. \end{aligned} \tag{15}$$

Of which, $a_m = m\pi f/2e$.

This level converges quickly, and a good approximate solution can be obtained by taking $m = 1$. Now, let the permafrost "plate cover" be a square plate with side length $2e$ in the inclined direction and length $2e$ in the strike direction, and the maximum deflection can be found at the center of the plate. Substituting $x = e$, $y = 0$, and $a = \pi/2$, into the above equation gives

$$\omega_{\max} = 0.0304 \frac{q_1 e^4}{D} = 0.0304 \frac{12(1 - U^2) q_t e^4}{E H_t^3}. \tag{16}$$

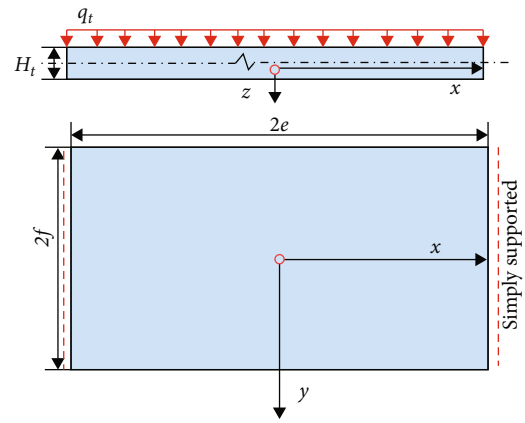

Figure 4: Mechanical model of suspended fracture.

It can be seen that the maximum tensile stress occurs at $z = -H_t/2$ at the lower end of the middle of the permafrost "slab cover," so that after the deformation of the permafrost "slab cover" on both sides in the inclined direction, the limit of the collapse distance in the inclined direction is reached, and the mechanical deformation will occur in the middle of the coal seam in the inclined direction. The mechanical deformation occurs in the middle of the seam.

2.2. Deformation Control Equations for Coal Rock Masses. The deformation control equation of a gas-bearing coal body consists of three parts: the stress balance equation, the geometric equation, and the intrinsic equation. The stress balance equation for a gas-bearing coal body is

$$\sigma_{ij,j} + F_i = 0, \tag{17}$$

where $\sigma_{ij,j}$ is the first-order partial derivative of the total stress component σ_{ij} of the coal rock body for the coordinates (i, j in the principal direction), N/m^3; F_i is the volume force component, N/m^3.

The geometric equation for the deformation of the coal rock body is:

$$\varepsilon_{ij} = \frac{1}{2}\left(u_{i,j} + u_{j,i}\right), \tag{18}$$

where ε_{ij} is the line strain component; $u_{i,j}$, $u_{j,i}$ are the first-order partial derivatives of the displacement components u_i, u_j, respectively, with respect to the coordinates.

From the generalized Hooke's law, the intrinsic equation of the coal rock body is obtained as shown in Equation (19), where G is the shear modulus of the coal rock body, MPa; E_v is the volume strain of the coal rock body; δ_{ij} is the Kronecker variable (1 for $i = j$, 0 for $i \neq j$); α_p is the Biot coefficient, and p is the gas pressure, MPa.

$$\sigma_{ij} = 2G\varepsilon_{ij} + \frac{2Gv}{1 - 2v}\varepsilon_V \delta_{ij} - \alpha_p p \delta_{ij}. \tag{19}$$

Combining Equations (17) to (19), the deformation control equation for coal rock masses considering pore pressure can be expressed in terms of displacement.

$$Gu_{i,jj} + \frac{G}{1-2\nu}u_{j,ji} - \alpha_p p + F_i = 0, \tag{20}$$

where $u_{i,jj}$, $u_{j,ji}$ are the second-order partial derivatives of the displacement components u_i, u_j for the coordinates, respectively.

2.3. Gas Transport Control Equations. The Langmuir isothermal sorption model is shown in

$$V_E(p) = V_L \frac{p}{p_L + p}, \tag{21}$$

where $V_E(p)$ is the adsorption volume, g/m^3; V_L is the Langmuir volume g/m^3; p_L is the Langmuir pressure, MPa, and the Langmuir pressure is the pressure at which the adsorption volume reaches 50% of the ultimate adsorption volume.

The fracture system of the coal body provides a channel for the free gas to deposit and seep through, and the mass balance equation of the gas in the fracture system of the coal body per unit volume is

$$\frac{\partial m_f}{\partial t} + \nabla\left(\rho_g q\right) = Q, \tag{22}$$

where m_f is the mass of free gas per unit volume of coal, kg/m^3; t is time, s; ρ_g is the gas density, kg/m^3; q is the Darcy velocity ignoring the effect of gravity, m/s; $q = -k\nabla p/\mu$, k is the coal permeability, m^2; μ is the gas dynamic viscosity, Pa•s; Q is the mass exchange rate between the matrix system and the fracture system per unit volume of coal, kg/(m^3•s).

Under isothermal conditions, the free gas content is only related to the gas pressure. According to the gas equation of state, the mass of free gas in a unit volume of gas-bearing coal can be obtained as

$$m_f = \varphi\rho_g = \varphi\frac{\rho_n}{p_n}p, \tag{23}$$

where φ is the porosity of the coal body, %; ρ_n is the density of gas at standard atmospheric pressure, kg/m^3; p_n is the standard atmospheric pressure, MPa.

The diffusion of gas in the coal body is mainly in the gas phase. According to the law of conservation of mass, the rate of change of gas mass per unit volume of coal matrix system with time is equal to the rate of mass exchange per unit volume of coal matrix system with the fracture system.

$$\frac{\partial m_\gamma}{\partial t} = -Q, \tag{24}$$

where m_r is the mass of adsorbed gas per unit volume of coal, kg/m^3. Considering the influence of moisture, ash, and combustible percentage in coal on gas adsorption, the mass of adsorbed gas per unit volume of coal can be obtained from the modified Langmuir equation, as shown in

$$m_\gamma = \frac{abp}{1+bp}\rho_g\rho_c\frac{100 - A - M}{100(1 + 0.31M)}, \tag{25}$$

where a is the ultimate gas adsorption capacity of the coal body, m^3/kg; b is the adsorption constant of the coal body, MPa^{-1}; ρ_c is the density of the coal body, kg/m^3; A is the ash content of the coal body, %: M is the moisture content of the coal body, %.

Let $R = \rho_g\rho_c((100 - A - M)/(100(1 + 0.31M)))$, then Equation (26) can be obtained

$$\frac{\partial(\varphi\rho_n p/p_n)}{\partial t} = \nabla\left(\frac{k\rho_n p}{\mu p_n}\nabla p\right) = -\frac{\partial(abpR/(1+bp))}{\partial t}. \tag{26}$$

2.4. Porosity and Permeability Evolution Equations. Coal porosity and permeability are the key coupling terms in the coupling of deformation field and gas transport field. By the definition of porosity, the coal porosity can be obtained by deducing that

$$\varphi = \frac{V_p}{V_B} = 1 - \frac{1-\varphi_0}{1+\varepsilon_v}\left(1 + \frac{\Delta V_s}{\Delta V_{s0}}\right), \tag{27}$$

where V_p is the pore volume, m^3; V_B is the coal body appearance volume, m^3; φ_0 is the initial porosity, %; ΔV_s is the change in coal body skeleton volume, m^3; ΔV_{s0} is the initial coal body skeleton volume change, m^3.

The volume deformation $\Delta V_s/\Delta V_{s0}$ includes the deformation $\Delta V_{sp}/\Delta V_{s0}$ caused by changes in gas pressure, the deformation $\Delta V_{sf}/\Delta V\Delta V_{s0}$ caused by the expansion of gas adsorbed by coal particles, and the deformation $\Delta V_{st}/\Delta V\Delta V_{s0}$ caused by the thermal expansion of coal skeletal particles.

$$\begin{aligned}\frac{\Delta V_s}{\Delta V_{s0}} &= \frac{\Delta V_{sp} + \Delta V_{sf} + \Delta V_{st}}{\Delta V_{s0}} \\ &= \frac{3(1-2\nu)}{E}\Delta p + \frac{\varepsilon_L p}{(p + p_L)(1-\varphi_0)} + \alpha\Delta T,\end{aligned} \tag{28}$$

where E is the modulus of elasticity of the coal body, GPa; Δp is the change in gas pressure, MPa; ε_L is the Langmuir volume strain constant; P_L is the Langmuir pressure constant, MPa; α is the volume expansion coefficient of the coal body, K^{-1}; ΔT is the absolute temperature change, K.

Considering the effects of gas pressure, coal rock volume strain, and temperature on porosity, the dynamic expression for the porosity of gas-bearing coal under isothermal conditions is derived as

$$\varphi = 1 - \frac{1-\varphi_0}{1+\varepsilon_V}\left[1 - \frac{3(1-2\nu)}{E}\Delta p + \frac{\varepsilon_L p}{(p + p_L)(1-\varphi_0)}\right], \tag{29}$$

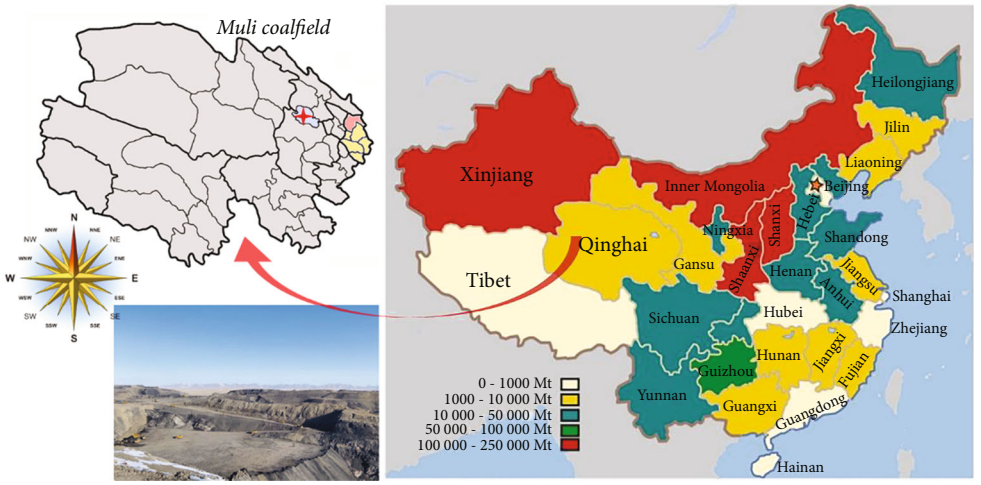

Figure 5: Illustration of the location of the Muli coalfield.

where φ_0 is the porosity of the coal body under the initial conditions; ε_V is the volume strain of the coal body under the corresponding gas pressure conditions.

Based on the Kozeny-Carman equation and defined by porosity and volumetric strain, this gives

$$\frac{k}{k_0} = \left(\frac{\phi}{\phi_0}\right)^3 = \frac{1}{1+\varepsilon_V(1+\beta)^2}\left(\frac{V_{p_0}+\Delta V_p}{V_{p_0}}\right)^3, \quad (30)$$

where k_0 is the initial coal body permeability, m^2; β is the ratio of the change in pore internal surface area to the initial internal surface area of the pore, which is much smaller than 1 and therefore negligible; V_{p0} is the initial pore volume of the coal body, m, and ΔV_p is the change in the pore volume of the coal body, expressed by the following equation:

$$\Delta V_p = \varepsilon_v V_{B0} - \left[\frac{\varepsilon_L p}{(1-\varphi_0)(P_L+p)} - \frac{3(1-2\nu)}{E}\Delta p\right] V_{s0}, \quad (31)$$

where V_{B0} is the initial appearance volume of the coal rock body, m^3; V_{S0} is the initial skeletal volume of the coal rock body, $V_{S0} = V_{B0} - V_{P0}$, m^3.

Let $\gamma = (\varepsilon_L p/(1-\varphi_0)(P_L+p)) - (3(1-2\nu)/E)\Delta p$ simplify the above equation to give

$$\frac{k}{k_0} = \frac{1}{1+\varepsilon_v}\left(1+\gamma+\frac{\varepsilon_V-\gamma}{\varphi_0}\right)^3. \quad (32)$$

The resulting equation for the dynamic evolution of coal body permeability is

$$k = k_0\left\{\frac{1}{\varphi_0} - \frac{1-\varphi_0}{\varphi_0(1+\varepsilon_V)}\left[1-\frac{3(1+2_V)}{E}\Delta p + \frac{\varepsilon_L p}{(p+P_L)(1+\varphi_0)}\right]\right\}^3. \quad (33)$$

2.5. Gas-Solid Coupling Model. Gas movement with the gas flow in confined space is essentially a single-phase multicomponent diffusion problem without chemical reaction. Its motion law satisfies the basic equations of fluid mechanics described by general Navier-Stokes equations, including continuity equation, momentum conservation equation, energy conservation equation, and component mass conservation equation. The control equations of coal and rock deformation and gas migration are unified to form a gas-solid coupling model. The couplings (8), (15), (19), (25), (28), and (32) together form a mathematical model for gas-solid coupling in the permafrost region close to the coal seam, see

$$\begin{cases} Gu_{i,jj} + \dfrac{G}{1-2\nu}u_{j,ji} - \alpha_p p + F_i = 0, \\ \dfrac{\partial(\varphi\rho_n p/p_n)}{\partial t} - \nabla\left(\dfrac{k\rho_n p}{\mu p_n}\nabla p\right) = -\dfrac{\partial(abpR/1+bp)}{\partial t}, \\ \varphi = 1 - \dfrac{1-\varphi_0}{1+\varepsilon_V}\left[1-\dfrac{3(1-2\nu)}{E}\Delta p + \dfrac{\varepsilon_L p}{(p+P_L)(1-\varphi_0)}\right], \\ k = k_0\left\{\dfrac{1}{\varphi_0} - \dfrac{1-\varphi_0}{1+\varepsilon_V}\left[1-\dfrac{3(1-2\nu)}{E}\Delta p + \dfrac{\varepsilon_L p}{(p+P_L)(1-\varphi_0)}\right]\right\}^3. \end{cases} \quad (34)$$

3. Project Case

The Muli coalfield is located in the alpine region of the northern Qinghai-Tibet Plateau, in the upper basin of the Datong River at the junction of Haibei Tibetan Autonomous Prefecture and Haixi Mongolian Tibetan Autonomous Prefecture in Qinghai Province, in the adjoining area of Tianjun, Gangcha, Qilian, and Haiyan counties in northern Qinghai Province, starting from Haiyan Pass in the east to the watershed of the Datong and Shule rivers in the west, bounded by the Datong and Tolai mountains in the north and south, respectively, including Jiangcang, Juhuqian, Hot Water, Arc Mountain, Waihi Hada, Haider, and Merle 7 mining areas a total of more than 20 well fields. It is shown as Figure 5.

The MNT coal mine is located on the south bank of the Datong River in the northeastern part of Qinghai Province and is the first large test shaft coal mine under construction in the Jiangcang mining area of Qinghai. The NMT coal mine has complex engineering conditions, and it is located in the permafrost area of Muli coalfield. The flake permafrost area of the NMT coal field accounts for 80% of the total area, and the permafrost layer is thick. The failure characteristics of the permafrost layer are different from ordinary strata, but continuous failure, with prominent creep mechanical characteristics. The minefield is approximately 3.47 km long from east to west and 1.81 km wide from north to south, covering an area of approximately 6.3 km^2, with a resource reserve of 212 Mt, a design production capacity of 1.2 Mt/a, and a design service life of 67 years. The mine is located in the high cold, low mountainous, and hilly area of the plateau, the ground elevation reaches about +3820~4000 m, the mine is located at an elevation of about +3850 m, the four seasons are not very distinct, the winter is very cold, the daily temperature difference is large, the lowest temperature is -34°C, the highest is 19.8°C, the average annual temperature is -4.2°C~5.1°CC, and it belongs to the continental climate of the plateau, the surface of the fourth system The strata are perennial permafrost layers that do not melt all year round.

The perennial permafrost in the Muli coalfield was formed during the Quaternary pale glacial period, and the neotectonic movement caused it to rise continuously, maintaining the alpine character and preserving the permafrost to this day. The permafrost in the coalfield is divided into a continuous permafrost distribution zone, a permafrost sheet distribution zone, and a permafrost island distribution zone. The perennial permafrost sheet distribution area is located between the snow line and 3,800 m below, and the MNT coal mine is located in this area. The perennial permafrost layer is found throughout the entire wellfield, and the Fourth Series strata are basically perennial permafrost layers.

The thickness of the MNT permafrost layer varies greatly, thickening from south to north and thinning from west to east, and the distribution pattern of the thickness of the Quaternary strata is roughly the same, except for the melt zone under the riverbed of Jiangcang, there is generally a distribution of multiyear permafrost layers ranging from about 30 to 80 m thick, and the thickness of the permafrost layer increases with the thickness of the Quaternary surface layer, with the thickest point close to 100 m, and the permafrost layer penetrates deeply into the bedrock. The thickness of the permafrost layer measured in some boreholes of the geological exploration construction is shown in Table 1, from which it can be seen that the maximum thickness of the multiyear permafrost layer is 89.15 m in hole 83 of exploration line 26, and the minimum thickness is 24.00 m in hole ZK28-1 of exploration line 28.

Combining the test results of mechanical parameters of permafrost specimens for many years and referring to the information about permafrost in the Qinghai area, physical composition, temperature, and water content of permafrost layer for many years, the mechanical parameters of the fourth series (Q) permafrost layer in NMT mine are: uniaxial compressive strength is 5.7 MPa, density 2000 kg/m^3, modulus of elasticity 2.7 GPa, Poisson's ratio 0.3, angle of internal friction 30%, cohesion 2 MPa, and tensile strength 1.63 MPa.

Table 1: Statistical table of the thickness of permafrost layer drilled in the NMT minefield.

Exploration line-number	The thickness of frozen soil (m)	Floor elevation of frozen soil (m)
29-90	84.25	3895.8
26-83	89.15	3780.0
25-85	53.20	3819.1
29-81	55.00	3829.5
ZK30-1	36.29	3823.9
ZK28-1	22.50	3851.9

A total of 8 coal seams are mined, divided into 2 groups, the upper coal group is nos. 2, 3, 4 (3 + 4), and 5 coal seams of the Shanxi Group, and the lower coal group is nos. 6, 8, and 9 coal seams. The main coal seams are nos. 3, 4, and 5, with average seam thicknesses of 1.15 m, 2.95 m, and 2.65 m, respectively. The seams contain a small number of intercalated gangue layers, all of which are stable and mineable in the whole area, with a minimum seam spacing of 5.6 m. Therefore, it is a typical close seam group mining, as shown in Figure 6.

There is a correlation between the gas content of the coal seam and the depth of burial of the coal seam, the thickness of the overlying bedrock, and the lithology of the top and bottom slabs. Therefore, I took coal samples from the main mining seam of the mine area during the first period to study the relationship between the coal seam gas content and the thickness of the overlying bedrock, and the burial depth of the coal seam as shown in Figure 7. As can be seen from Figure 7, the gas content of the coal seam has a linear relationship with the depth of burial of the coal seam and the thickness of the overlying bedrock, but as the depth of burial of the south wing coal seam in the mine area is generally greater than that of the north wing coal seam, the gas content of the south wing coal seam is generally higher than that of the north wing coal seam under the same coal seam base elevation conditions.

The pore distribution characteristics of the coal seams in the mine area are shown in Table 2, the largest proportions of medium, micropores, and small pores are in coal seams 3#, 4#, and 5#, accounting for 83.57%, 66.31%, and 69.57% of the total pores, while the main flow places of gas in the coal seams are visible pores, large and medium pores, and micropores, and small pores are the main storage spaces for adsorbed gas. The mechanical properties of the rock and coal seams are shown in Table 3.

4. Results and Discussion

According to the definition of the thin plate theory, when the ratio of the thickness of the plate to the minimum width is greater than 1100-1/80 and less than 1/8-1/5, it can be regarded as a thin plate. It is in a large area of

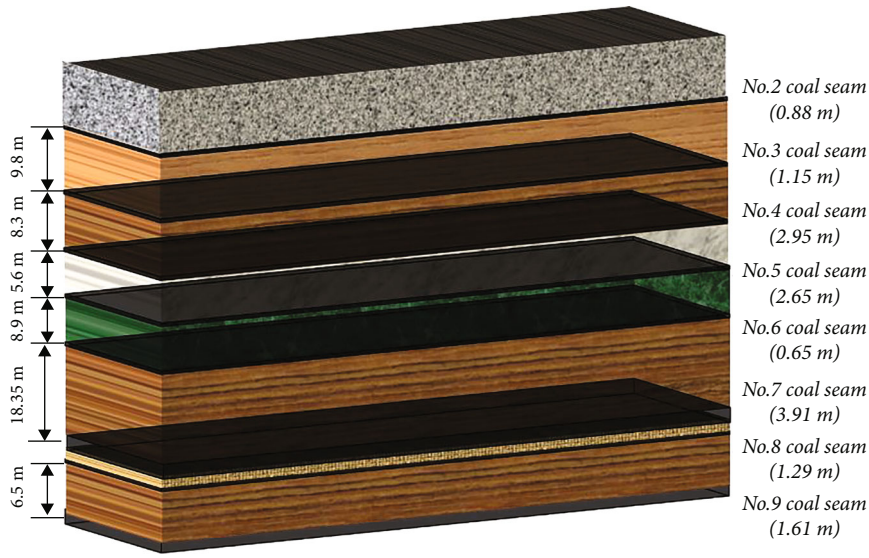

Figure 6: Coal seam distribution map.

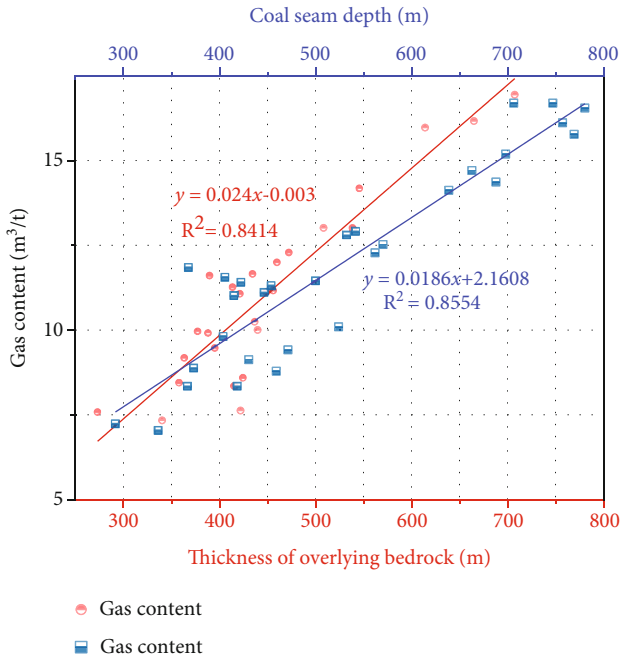

Figure 7: Relationship between the gas content of the coal seam and the thickness of the overlying bedrock and depth of burial of the coal seam.

overhang, which is consistent with the elastic thin plate theory. Therefore, the deformation characteristics and movement patterns of the tundra crust can be analyzed using the thin plate theory.

Based on the established theoretical model, it can be seen that in the mining of the large inclined coal seam group under the permafrost layer in the NMT coal mine, the tilting and rotating composite roof structure of the roof slab has caused tensile damage at the two ends and the middle of the tilting direction of the permafrost layer "slab cover," although it cannot form a macroscopic fracture phenomenon, with its continuous tilting. The left and right sides of the tilted direction and the central part of the tilted direction will be fractured by cracks. The permafrost "slab cover" in the direction of the strike forms a thick slab that is similar to the left and right ends of the break free, while the work is supported in the front and rear directions, at which point the permafrost "slab cover" can be seen as a thick strip beam structure in the direction of the strike. The collapse of the permafrost "slab cover" in the direction of travel is mainly caused by its own gravity.

In the initial stage of mining of the large dip coal seam group under the permafrost layer in the NMT coal mine, the permafrost layer does not have a delamination structure with its lower part, or the delamination structure is small; the permafrost layer is more integral and has a higher tensile and shear strength. The perennial permafrost "slab cover" does not break down near the midpoint of the long and short supports. As the coal seam is mined and the protective rock beam is formed, the structure becomes more complex as the overhang distance increases and the forces on the permafrost "slab cover" become more complex. The slab cover is a composite structure with a perennial permafrost layer, creating a delaminated structure.

According to the results of the theoretical analysis, there is a mechanical coupling relationship between the mechanical damage of the permafrost "slab cover" and the breakage of the lower coal rock body. The main relationship is: the rotational tilting movement of the protective rock beam will produce stress on the left support point of its tilting direction, and the supporting rock will have a tendency to move to the left, forming tensile stress on the upper part of the overlying ground surface of the permafrost layer "slab cover," driving its overall tilting direction to the left. As the lower part of the permafrost layer "plate cover" is suspended, its own gravity sinks and bends to form tensile stresses on both sides of the permafrost layer, which is balanced by tensile stresses on the right side of the inclination. In the direction of the working face, the perennial permafrost layer "plate cover" due to its own gravity in the direction of both

Table 2: Pore distribution characteristics.

Coal seam	Micropore		Pinhole		Mesopore		Macropore		Ss	φ/%
	V_s/(mL/g)	φ_s/%	V_p/(mL/g)	φ_0/%	V_p/(mL/g)	φ_0/%	V_p/(mL/g)	φ_0/%		
3#	0.0165	56.51	0.0079	27.06	0.0014	4.79	0.0034	11.64	3.756	3.55
4#	0.0259	43.55	0.0136	22.76	0.0095	15.90	0.0103	17.27	3.893	2.68
5#	0.0227	45.04	0.0123	24.53	0.0091	17.97	0.0069	11.61	2.455	3.53

Note: V_s: pore volume per unit mass, φ_s: specific pore volume, Ss: specific surface area.

Table 3: Characteristic parameters of coal seam and rock stratum.

Parameter	Rock stratum			Coal seam		
	Direct roof	Waste inclusion	Direct base plate	3#	4#	5#
E /GPa	23.1	15.2	21.9	4.7	4.1	3.3
c /MPa	3.1	3.2	1.5	3.3	3.0	2.8
Φ/°	33.2	31.7	37.8	24.1	23.9	23.8
υ	0.24	0.20	0.24	0.32	0.30	0.29
ρ/(kg/m^3)	2610	2690	2690	1320	1338	1350
a/(m^3/kg)	/	/	/	9.9×10^{-3}	11.0×10^{-3}	13.0×10^{-3}
0	/	/	/	9.6×10^{-18}	9.2×10^{-18}	9.0×10^{-18}
p_0/MPa	/	/	/	1.2	1.3	1.5
μ/(Pa•s)	/	/	/	1.08×10^{-6}	1.08×10^{-6}	1.08×10^{-6}
A/%	/	/	/	0.97	1.05	1.09
M/%	/	/	/	15.91	12.31	9.86
P_L/MPa	/	/	/	0.52	0.58	0.69
L	/	/	/	0.01	0.01	0.01

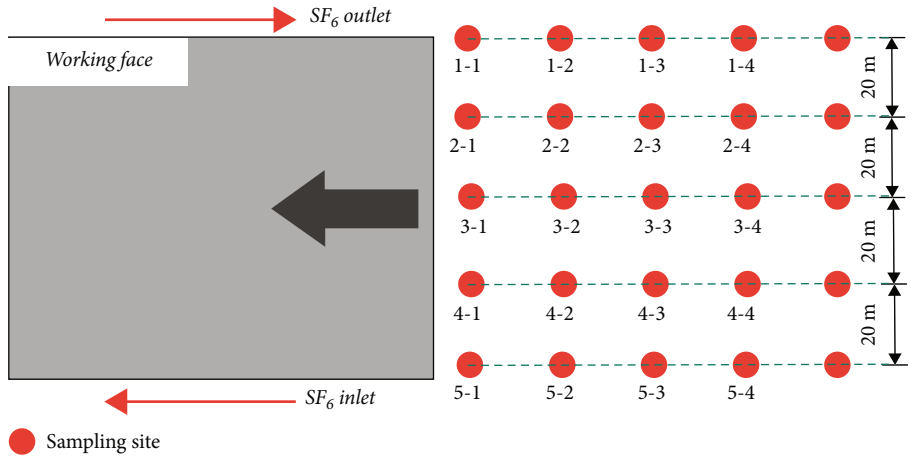

Figure 8: Arrangement of gas sampling points in the mining area of the working face.

sides of the tensile stress for the perennial permafrost layer "plate cover" above the force is uniform. There is also a tendency to move to the left of the dependent works, resulting in widespread tensile damage near the fixed boundary at the right end of the mechanical model.

In this paper, the mathematical model is established based on theoretical analysis, and the boundary conditions are given with the field test data. Then, the parameters are inversely calculated by the Matlab software. As the working face progresses, when the permafrost "slab cover" overhang distance 1 reaches the initial collapse step L_c, $x = 0$, $z = H_t/2$, σ_x reaches the permafrost ultimate tensile stress subject to the maximum tensile stress σ_t, thus obtaining the initial permafrost "slab cover." The first step across the break is calculated by

$$L_c = H_t\sqrt{\frac{4[\sigma_t] + q_t(4+3\nu)}{q_t}} = H_t\sqrt{\frac{4[\sigma_t] + \gamma_t H_t(4+3\nu)}{\gamma_t H_t}}. \quad (35)$$

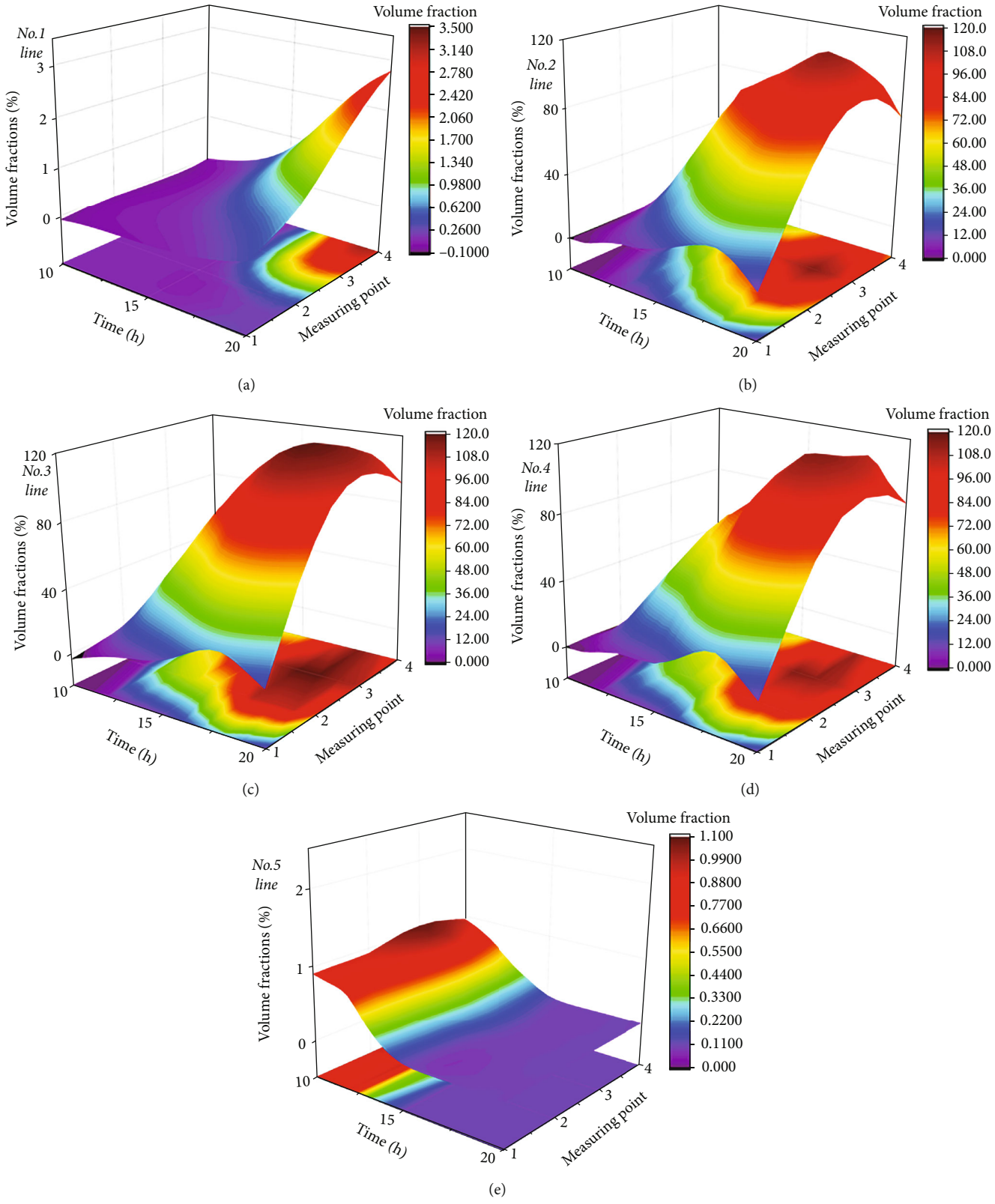

Figure 9: Gradient diagram of SF_6 concentration changes in the mining area of the working face.

After the initial span break of the permafrost layer, a cantilever beam structure is formed, and with the continuous advance of the working face direction, when the overhang distance 1 reaches the initial collapse step L_z, $x = 0$, $z = -H_t/2$, σ reaches the permafrost ultimate tensile stress subject to the maximum tensile stress σ_t, thus obtaining

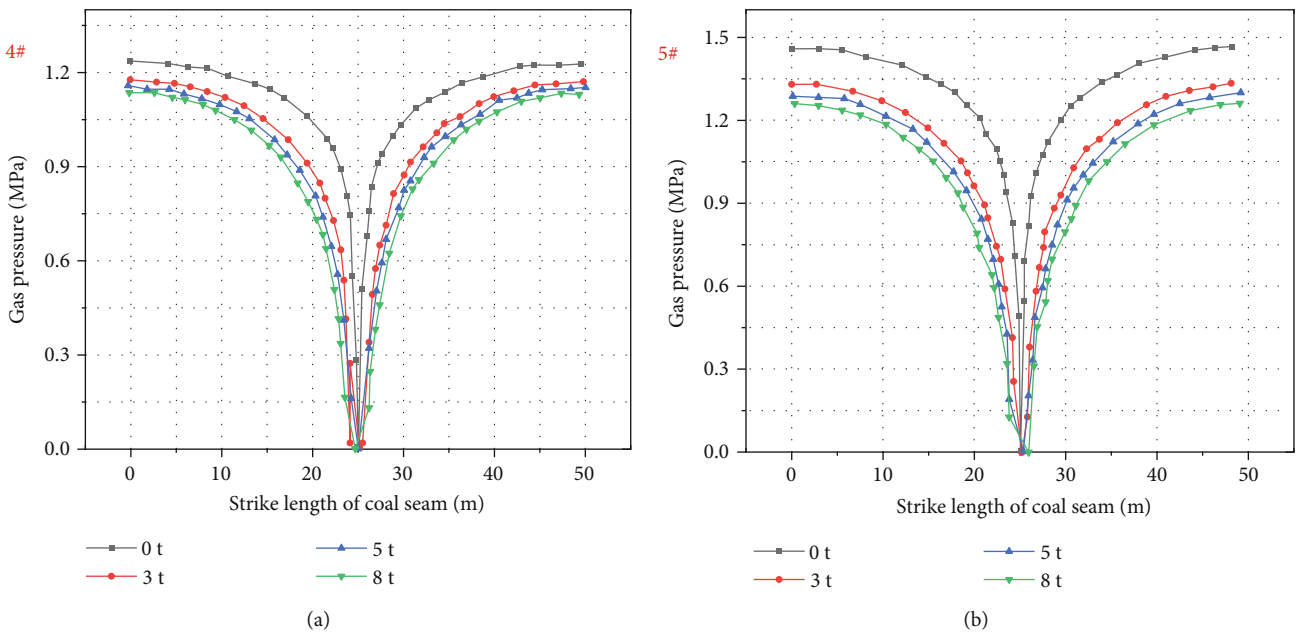

Figure 10: Variation of gas pressure at different coal output after 60 d of extraction.

the permafrost "plate cover" cycle span break step

$$L_s = H_t\sqrt{\frac{[\sigma_t] + (1/5)q_t}{3q_t}} = \sqrt{\frac{([\sigma_t] + (1/5)\gamma_t H_t)H_t}{3\gamma_t}}. \quad (36)$$

Substituting the mechanical parameters of the Quaternary (Q) permafrost layer at the NMT mine, based on an average permafrost thickness of 60 m, the initial collapse step in the strike direction and the periodic collapse step are

$$L_c = 60 \times \sqrt{\frac{4 \times 1630000 + 20000 \times 60 \times (4 + 3 \times 0.3)}{20000 \times 60}} = 192.87m,$$
$$L_s = \sqrt{\frac{(1630000 + (1/5) \times 20000 \times 60) \times 60}{3 \times 20000}} = 43.24m. \quad (37)$$

In comparison to the initial and periodic collapse steps for general geological conditions, the perennial permafrost has significantly larger values for the initial and periodic collapse steps due to its low density and high tensile strength, which requires attention in coal mining practice. As the lower part of the permafrost, the crust is less detached, and the deformation breakage of the permafrost cover is also minimal and does not cause damage to water resources or surface ecology.

The stress field-fissure field evolution and distribution characteristics of the overburden studied indicate that coal seam clusters are likely to produce large fissures or penetrating fissures under stacked mining conditions; however, the fissure penetration between coal seams has an important influence on the determination of gas transport and extraction parameters. Therefore, to investigate the gas transport and enrichment characteristics of the proximal coal seam

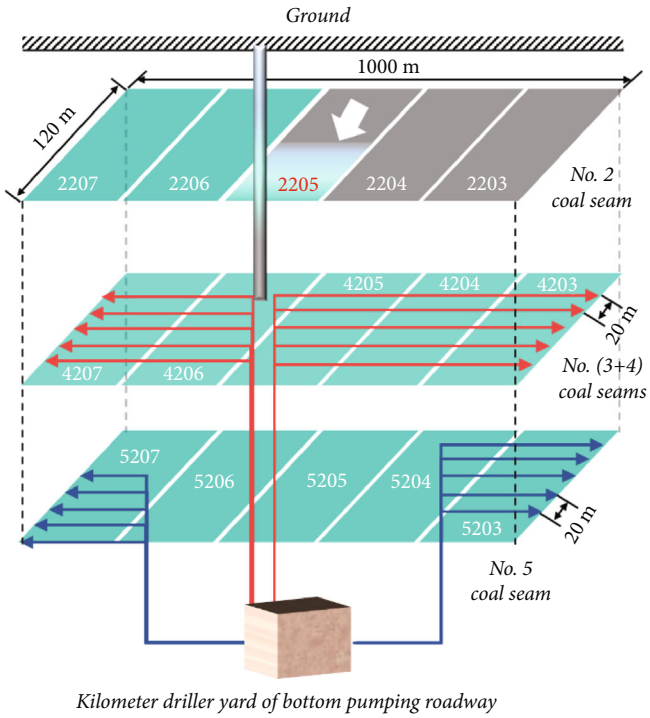

Figure 11: Design of directional drilling group prepumping in protective layer mining + floor extraction roadway.

group under stacked mining conditions, SF_6 tracer gas identification was used to verify the penetration of interseam fissures and the degree of influence of penetrating fissures in the field.

The test site was the underground drilling site of the return tunnel of the (3#+4#) coal seam, the target coal seam was the (3#+4#) coal seam, the sampling site was the extraction area of the working face of the no. 2 coal seam and the

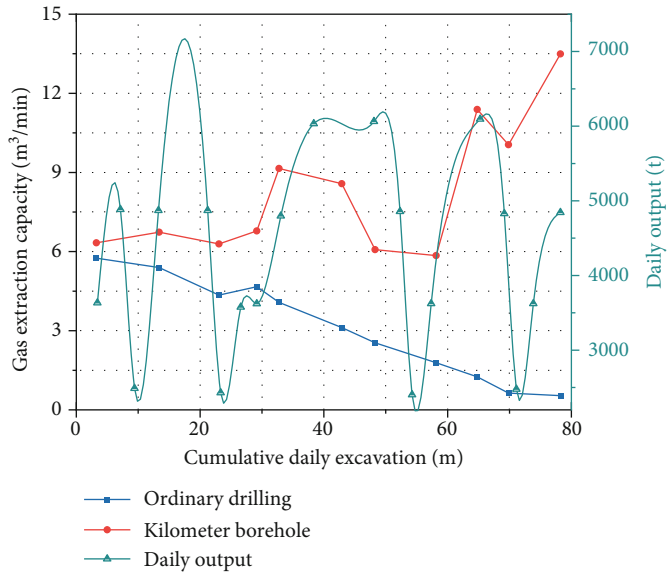

Figure 12: Gas drainage pure volume comparison of directional drillings and ordinary through layer drillings.

gas extraction borehole of the (3#+4#) coal seam; 5# measurement lines were arranged at the 2# ends of the working face and the floor of the extraction area, respectively, and gas samples were collected utilizing preburied pipes, as shown in Figure 8.

As SF_6 gas was found on the measurement lines in the mining area of the no. 2 coal face, it indicates that a penetration fissure had been created between the no. 2 coal face and the (3#+4#) coal face at this time; no SF_6 gas was found in the first nine gas retrievals, but SF_6 was found in the 10th gas retrieval, indicating that the face was mined back to the position at the time of the 10th gas retrieval, and a penetration fissure was created between the no. 2 coal face and the (3#+4#) coal face. SF_6 gas was first detected at measurement points 2-3 and 4-3, respectively, indicating that a floor penetration-type fissure was generated at a location 30-40 m behind the protective seam workings. From the three-dimensional map of SF_6 time concentration distribution in the mining area, it can be seen that according to the time when SF_6 gas was first detected at measurement points 2-3 and 4-3 and the distance the working face advanced at this time, it indicates that the interseam penetration fissure was generated at about 40 m behind the working face of coal seam no. 2, and then, SF gas was also detected at other measurement points (measurement points 2-2, 2-4, 4-2, and 4-4) at the same time. This indicates that not only did the (3#+4#) seam produce a penetration fissure but also that secondary fissures were developed in its vicinity, and that SF_{66} gas originating from the (3#+4#) seam was transported through the penetration fissure to the area 20-60 m behind the working face of the no. 2 seam. The result are shown as Figure 9.

Therefore, according to the mining stress evolution-fissure development-gas transport characteristics under the overlapping mining conditions of the close coal seam group, it is found that the effect of overlapping mining on the overburden stress field and fissure field is not a simple superposition of effects, but a "1 + 1 > 2" effect, so that the overburden coal seam produces penetrating fissures under the overlapping mining, and a large number of secondary fissures are derived around it, which timely provides a superior channel for coal seam gas. This provides an advantageous channel for the transport of coal seam gas.

Based on the requirement of "simultaneous management" of coal seam gas and protrusion hazards, the finite difference method was used for the two close coal seams 4# and 5# based on the established gas-solid coupling model. The gas pressure variation under different coal discharge (unloading) conditions at the same time were analyzed. The pressures at the boreholes in the 4# and 5# seams were calculated for coal volumes of 0, 3, 5, and 8 t, respectively. The gas pressure distribution at the calculation point after 60 d of extraction is shown in Figure 10.

From the calculation results, it can be seen that under the condition of constant extraction time, the effective radius of influence of extraction is proportional to the amount of coal produced. At a certain extraction time, the coal output from the 4# coal seam is 0, 3, 5, and 8 t, respectively, and the gas pressure 0.74 MPa isopotential line is 1.65, 5.12, 7.30, and 8.06 m from the borehole wall, respectively, while the coal output from the 5# coal seam is 0, 3, 5, and 8 t, respectively, and the gas pressure 0.74 MPa isopotential line is 0.86, 2.55, 3.91, and 4.40 m from the borehole wall, respectively. This shows that the larger the coal output, the larger the effective radius of influence and the better the gas extraction effect. However, in the actual construction process, in order to ensure safety during the recovery period, the amount of coal exiting should not be too large.

To break through the problem of gas extraction from close coal seams and realize the comining of coal and gas in a multiseam three-dimensional area, this paper proposes the "Protected Seam Mining + Directional Drilling Group in Bottom Extraction Lane Comining Technology" based

on the spatial and temporal conditions and requirements of coal-gas comining at different stages, which can release high-quality coal and coal-bed methane production capacity while ensuring safe production in mines.

In a mining area of the mine, for example, the no. 2 coal seam is used as a protective layer to mine a total of 5 working faces from 2203 to 2207 (Figure 11), and the no. 2 bottom extraction road is arranged in the bottom plate of the no. 5 coal seam below the 2205 working face; the length of the roadway is 1284 m. 10 drilling fields (10 directional holes) are arranged in the north and south of the roadway, and a group of an upward directional hole is constructed along the coal seam, with a hole diameter of 113 mm, hole The final hole height is located in the no. 3 + 4 and no. 5 coal seams, respectively, each covering 5 working faces corresponding to the upper and lower coal of these 2 seams, and the no. 2 coal seam adopts 120 mm large hole diameter progressive presumping.

Statistical analysis of the pure extraction volume of the 1,000 m drill hole and the common through seam drill hole in the 4203 working face of the second mining area shows that the pure volume of the 1,000 m drill hole is 5.05~10.88 m/min^3, which is about 2.5 times of the common through the seam drill hole, and the pure volume of the common drill hole gradually decreases as the working face advances, while the extraction volume of the long directional drill hole is basically greater than 6 m/min. The daily production of the working face was increased from 4850 $t^3$to 6100 t, an increase of 25.8%, and both coal and CBM production were significantly increased. The gas drainage pure volume comparison of directional drillings and ordinary through layer drillings are shown as Figure 12.

On the one hand, the paper reveals the fracture forms, failure characteristics, and spatial structure relationship of coal roof and permafrost during the mining process of coal seam group with large dip angle under permafrost overburden. On the other hand, it is necessary to observe and study the permafrost surface deformation in the next production practice to verify the correctness of the research conclusions. The stability control of overlying rock in the mining of coal seam with large dip angle under the permafrost layer needs further study.

5. Conclusions

In this paper, a theoretical model of small deflection of thin plate is established based on Kirchhoff's assumptions, and the deformation characteristics of the "cover" layer in the permafrost zone are analyzed; a gas-solid coupling model is derived and established for the close coal seam gas-integrated mining face, and the following conclusions are obtained for the NMT coal mine.

(1) There is a tendency for the multiyear permafrost layer at the NMT mine to move to the left, which will produce extensive pulling damage near the right end. The initial and periodic collapse steps are 192.87 m and 43.24 m, respectively, which are significantly larger than the initial and periodic collapse steps under normal geological conditions but will not cause damage to water resources or surface ecology

(2) The pore and fissure structural characteristics of the coal seams in the NMT mine are not conducive to gas transport. The effect of overburden mining on the overburden stress and fissure fields is not a simple superposition of effects, but a nonlinear incremental effect, with penetrating fissures generated under overburden mining and a large number of secondary fissures derived in the surrounding area, which provide an advantageous channel for coal seam gas transport in time

(3) Based on the established gas-containing gas-solid coupling model, the gas pressure evolution characteristics of the proximity coal seam are analyzed. The results show that under the condition of constant gas extraction time, the effective influence radius of extraction is directly proportional to the coal output. The larger the coal output, the larger the effective radius of influence and the better the gas extraction effect

(4) Given the difficulties of gas extraction, based on the spatial and temporal conditions and requirements of coal-gas comining in different stages, the "protected layer mining and bottom extraction lane directional drilling group comining technology" was proposed. Both coal and CBM productions were significantly increased

Data Availability

The data used to support the findings of this study are available from the corresponding author upon request.

Conflicts of Interest

The authors declare that they have no known competing financial interests or personal relationships that could have appeared to influence the work reported in this paper.

References

[1] H. G. Zhang, "Experimental study on freeze-thaw damage of soft interlayer in opencast coal mine in high altitude permafrost area," *Journal of Xi'an Technological University.*, vol. 39, no. 4, pp. 408–413, 2019.

[2] C. Liu, Y. Wang, X. Hu, Y. Han, X. Zhang, and L. Du, "Application of GA-BP neural network optimized by Grey Verhulst model around settlement prediction of foundation pit," *Geofluids*, vol. 2021, 2021.

[3] S. H. Xu, N. Li, X. D. Wang et al., "Damage test and degradation model of saturated sandstone due to cyclic freezing and thawing of rock slopes of the open-pit coal mine," *Chinese Journal of Rock Mechanics and Engineering*, vol. 35, no. 12, pp. 2561–2571, 2016.

[4] L. Q. Tang, D. X. Nie, D. Y. Liu, and Y. U. Xianhua, "Analysis of main factors influencing strength parameters of soft

intercalation," *Journal of Engineering Geology*, vol. 20, no. 2, pp. 289–295, 2012.

[5] W. Xiang, "The study of microstructures of weak intercalations and their mechanical significance," *Earth Science-Journal of Wuhan College of Geology*, vol. 10, no. 1, p. 165, 1985.

[6] W. X. Fu, D. X. Nie, Y. Q. Shang, and Y. M. Chen, "Study on engineering properties of weak layers under ground stresses," *Chinese Journal of Geotechnical Engineering*, vol. 24, no. 5, pp. 584–591, 2002.

[7] M. W. X. X. Z. Lixin, "Influence of frost and thaw cycles on shear strength of lime silt," *Chinese Journal of Geotechnical Engineering*, vol. 21, no. 2, pp. 158–163, 1999.

[8] C. S. Yang, P. He, G. D. Cheng, Z. Yuanlin, and Z. Shuping, "Testing study on influence of freezing and thawing on dry density and water content of soil," *Chinese Journal of Rock Mechanics and Engineering*, vol. 22, no. S2, pp. 2695–2699, 2003.

[9] T. L. Han, Y. S. Chen, and J. P. Shi, "Experimental study on mechanical properties and damage degradation mechanism of calcareous sand-stone subjected to freeze-thaw cycles," *Chinese Journal of Geotechnical Engineering*, vol. 38, no. 10, pp. 1802–1812, 2016.

[10] J. M. Konrad, "Physical processes during freeze-thaw cycles in clayey silts," *Cold Regions Science and Technology*, vol. 16, no. 3, pp. 291–303, 1989, (in Chinese).

[11] R. N. Yong, "Alteration of soil behaviour after cyclic freezing and thawing," *International Symposium On Ground Freezing*, vol. 4, pp. 187–195, 1985.

[12] W. Tian, Y. L. Xie, and F. N. Dang, "Experimental study on the mechanical property and damage evolution of concrete under freeze-thaw environment," *Journal of Sichuan University*, vol. 47, no. 4, pp. 38–44, 2015.

[13] Z. H. Cheng, Q. X. Qi, H. Y. Li, L. Zhang, and X. G. Liu, "Evolution of the superimposed mining-induced stress-fissure field under extracting of close distance coal seam group," *Journal of China Coal Society*, vol. 41, no. 2, pp. 367–375, 2016.

[14] Z. H. Cheng, S. L. Su, and X. Wang, "Study on mining-induced fracture field of contiguous coal seam with BBM-DEM simulation," *Coal Science and Technology*, vol. 47, no. 12, pp. 1–9, 2019.

[15] Q. X. Qi, Z. H. Cheng, L. Zhang et al., "Analysis on the feasibility of upper protective layers mining in contiguous seams with coal and gas outburst hazard," *Coal Science and Technology*, vol. 43, no. 4, pp. 43–47, 2015.

[16] H. F. Ma, Z. H. Cheng, and W. Liu, "Evolution characteristics of mining stress and overlying strata displacement field under superimposed mining in close distance coal seam group," *Journal of Safety Science and Technology*, vol. 13, no. 5, pp. 28–33, 2017.

[17] J. Li, Z. Jiao, M. Zhang, and Y. Li, "Dynamic evolution characteristics and mechanism of surrounding rock fractures during the repeated mining of closed distance deep coal seam," *Revista International DE Contamination Ambiental*, vol. 1, no. 35, pp. 165–176, 2019.

[18] J. Ning, J. Wang, Y. Tan, and Q. Xu, "Mechanical mechanism of overlying strata breaking and development of fractured zone during close-distance coal seam group mining," *International Journal of Mining Science and Technology*, vol. 30, no. 2, pp. 207–215, 2020.

[19] J. L. Xu and M. G. Qian, "Study and application of mining-induced fracture distribution in green mining," *Journal of China University of Mining& Technology*, vol. 33, no. 2, pp. 141–144, 2004.

[20] M. G. Qian, J. L. Xu, and X. X. Miao, "Green technique in coal mining," *Journal of China University of Mining & Technology*, vol. 32, no. 1, pp. 343–347, 2003.

[21] D. J. Xue, H. W. Zhou, X. L. Tang, and Y. F. Zhao, "Evolution of mining-induced enhancement and distribution of gas permeability in coal seam and surrounding rock," *Journal of China Coal Society*, vol. 38, no. 6, pp. 930–935, 2013.

[22] D. J. Xue, H. W. Zhou, T. Zhao, J. Y. Ding, and C. Li, "Algorithm of fractal dimension of rock fracture surface based on volume estimation," *Chinese Journal of Geotechnical Engineering*, vol. 34, no. 7, pp. 1256–1261, 2012.

[23] H. Zhou, J. Liu, D. Xue, H. Yi, and J. Xue, "Numerical simulation of gas flow process in mining-induced crack network," *International Journal of Mining Science and Technology*, vol. 22, no. 6, pp. 793–799, 2012.

[24] Y. Xue, J. Liu, X. Liang, S. Wang, and Z. Ma, "Ecological risk assessment of soil and water loss by thermal enhanced methane recovery: numerical study using two-phase flow simulation," *Journal of Cleaner Production*, vol. 334, article 130183, 2022.

[25] Y. Cheng, Q. Liu, and T. Ren, *Coal Mechanics*, Springer Singapore, 2021.

[26] Q. X. Yu, Y. P. Cheng, C. L. Jiang, and S. N. Zhou, "Principles and applications of exploitation of coal and pressure relief gas in thick and high-gas seams," *Journal of China University of Mining & Technology*, vol. 32, no. 2, pp. 128–131, 2003.

[27] Y. P. Cheng, Q. X. Yu, and L. Yuan, "Gas extraction techniques and movement properties of long-distance and pressure relief rock mass upon exploited coal seam," *Journal of Liaoning Technical University*, vol. 22, no. 4, pp. 483–486, 2003.

[28] L. Yuan, "Key technology for the simultaneous extraction of coal gas in low permeable high gas content coal seam cluster under pillarless gob side entry retained with Y type ventilation," *China Coal*, vol. 34, no. 6, pp. 9–13, 2008.

[29] L. Yuan, H. Guo, B. T. Shen, Q. D. Qu, and J. H. Xue, "Circular overlying zone at longwall panel for efficient methane capture of multiple coal seams with low permeability," *Journal of China Coal Society*, vol. 36, no. 3, pp. 357–365, 2011.

[30] X. Q. Fang, Y. Q. Geng, and M. Wang, "Kilometer directional drilling: simultaneous extraction of coal and gas from a high gas coal seam," *Journal of China University of Mining& Technology*, vol. 41, no. 6, pp. 26–33, 2012.

[31] Z. W. Wang, K. Ma, H. Y. Tian et al., "Numerical analysis on time delay law and its influence factors of stress wave propagation through cracks," *Coal Science and Technology*, vol. 47, no. 6, pp. 66–72, 2019.

[32] Y. Xue, J. Liu, P. G. Ranjith, Z. Zhang, F. Gao, and S. Wang, "Experimental investigation on the nonlinear characteristics of energy evolution and failure characteristics of coal under different gas pressures," *Bulletin of Engineering Geology and the Environment*, vol. 81, no. 1, p. 3, 2022.

[33] C. Liu, L. Du, X. Zhang, Y. Wang, X. Hu, and Y. Han, "A New Rock Brittleness Evaluation Method Based on the Complete Stress-Strain Curve," *Lithosphere*, vol. 2021, no. Special 4, article 4029886, 2021.